Asian Journal of Chemistry; Vol. 35, No. 3 (2023), 617-623

ASIAN JOURNAL OF CHEMISTRY

https://doi.org/10.14233/ajchem.2023.27482

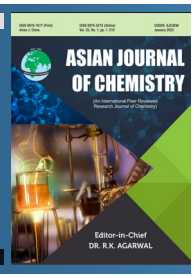

Design, Synthesis, Anti-tubercular and Docking Studies of Novel 2-Furanyl-3-substituted Quinazolin-4-one Derivatives

RAJASEKHAR KOMARLA KUMARACHARI*, MAYANDIGARI GURUVAREDDY, M. PHEBE, PUTTAREDDY LOKESWARI REDDY, MARELLA SAI NITHIN, DESINGU LAKSHMIPATHI and MADDALI MANASA

Department of Pharmaceutical Chemistry, Sri Padmavathi School of Pharmacy, Tiruchanur, Tirupati-517503, India

*Corresponding author: Fax: +91 877 2237732; E-mail: komarla.research@gmail.com

Received: 29 December 2022; *Accepted*: 24 January 2023; *Published online*: 27 February 2023; AJC-21153

In this work, the synthesis, characterization and the anti-tubercular activity of novel 2-furanyl-3-substituted quinazolin-4-one derivatives and also predicted their affinity against *Mycobacterium tuberculosis* enoyl acyl carrier protein reductase were carried out. The targeted compounds were synthesized by the condensation of 2-(furan-2-yl)-4(3*H*)-1-benzoxazine-4-one with different primary amines. After structural elucidation using spectral data, the compounds were screened for anti-tubercular activity against *Mycobacterium tuberculosis* $H_{37}RV$ strain. The binding affinity against enoyl acyl carrier protein reductase was predicted using MOE and FITTED docking tools. The synthesized compounds showed a promising anti-tubercular activity in the range from 12.5 to 100 µg/mL. According to MOE docking, the common amino acids in the active site of InhA were found to form hydrogen bonding and hydrophobic interactions with the synthesized quinazolinones. Docking simulations also showed that an aromatic side chain capable of forming hydrogen bond interactions can increase affinity of 2-furanyl quinazolinones to enoyl acyl carrier protein reductase.

Keywords: Quinazolinones, Anti-tubercular activity, *Mycobacterium tuberculosis*, Docking studies.

INTRODUCTION

Globally, the number of deaths attributable to tuberculosis is decreasing, but not quickly enough to meet the target of a 35% decrease between 2015 and 2020. The global burden of tuberculosis has been declining recently, but the COVID-19 pandemic could undo those gains. As many as 0.2-0.4 million additional people could lose their lives to tuberculosis in year 2020. One factor in the rise in TB mortality is the spread of strains of tuberculosis which are resistant to several drugs, such as MDR-TB and XDR-TB. The MDR-TB was estimated to have caused the deaths of approximately 190,000. In the MDR-TB population, XDR-TB affects an estimated 9.7% of patients [1]. To make the conditions even worse, totally drug resistant TB (TDR-TB) has emerged over several countries, no effective treatment options exist for those patients as the strain is resistant to all available anti-TB drug [2-8]. Those reports necessitated an increased medicinal chemists' effort in the discovery and development of novel anti-tubercular agents.

A review of the literature highlighted the wide range of biological actions exhibited by quinazolinone derivatives. The antimicrobial, antiviral, antifungal, anti-allergic, antitumor, and antimycobacterial activities of quinazolinones have been well-documented [9-12]. Recently, the synthesis and antibacterial and antitubercular activity of certain 2,3-disubstituted quinazolinone derivatives [13] has been reported.

In this work, six novel 2-furanyl-3-substituted quinazoline-4-one derivatives (**6a-f**) were synthesized and their anti-tubercular efficiacy were investigated. Several compounds with different i*n vitro* anti-tubercular activity were synthesized by changing the substitution at the 3-position of 2-furanyl quinazolin-4-one. The binding affinity of the synthesized quinazolinone deriv-atives towards the enzyme (InhA) was predicted using docking studies. This will help to determine whether a relationship exists between binding affinity to InhA and minimum inhibitory concentration (MIC) for quinazolinone based anti-tubercular drugs. The *Mtb* enoyl acyl carrier protein reductase (InhA) is an enzyme of the mycobacterial FAS-II system that catalyses the NADH-dependent reduction of the *trans*-double bond between sites C2 and C3 of fatty acyl substrates [14]. The main target of the anti-tubercular drug

isoniazid is inactive inhA [15]. However, resistance to isoniazid is on the rise; as much as 30% of all *Mtb* clinical isolates are resistant to isoniazid [16]. The development of new InhA inhibitors may prove useful in combating MDR-TB and XDR-TB that have developed resistance to isoniazid. In light of this, docking studies were performed using *Mtb* InhA and the synthetic molecules.

EXPERIMENTAL

The chemicals used in this work were procured from the reputed commercial sources and used without further purfication. The melting points were determined in an open capillary tube using digital melting point apparatus and are uncorrected. Using cyclohexane:ethyl acetate (2:1), TLC was used to determine the homogeneity and purity of the compounds on silica gel GF-254 plates. The infrared spectra were recorded on a Shimadzu FT-IR 6000 using KBr discs. The Perkin-Elmer Series II 2400 CHNS/O Elemental Analyzer was used to conduct the CHNO elemental analysis. Direct insertion probe method was used to obtain mass spectra on the JEOL GC Mate II GC-Mass spectrometer at 70 eV. With a BRUKER AVIII-500 MHz FT-NMR spectrometer, ^{1}H NMR spectra were recorded using DMSO-d_6 as solvent and TMS as internal standard.

General synthetic procedure of 2-(furan-2-yl)-4(3*H*)-substituted quinazolin-4-ones (6a-f): Anthranilic acid (**2**, 0.01 mol) dissolved in pyridine (30 mL) was added dropwise to furoyl chloride (**1**) and then the reaction mixture was stirred for 2 h at room temperature. Upon cooling the solution, cold conc. HCl was added and then the obtained solid was filtered, washed thoroughly with distilled water and finally recrystallized with ethanol to get *N*-(2-acetylphenyl)furan-2-carboxamide (**3**). The progress of the reaction was monitored by TLC using cyclohexane:ethyl acetate (2:1) as mobile phase.

In next step, compound **3** (0.01 mol) and acetic anhydride (0.1 mol) were refluxed for 4 h before the solvent was extracted under reduced pressure. Petroleum ether was used to triturate the residue. To obtain 2-(furan-2-yl)-4(3H)-1-benzoxazin-4-one (**4**), the separated solid was then recovered by filtration, washed with petroleum ether, dried and re-crystallized with ethanol. Using TLC, the cyclohexane:ethyl acetate (2:1) as mobile phase, the completion of the reaction was established.

In final step, the reaction mixture of compound **4** (0.01 mol) and primary amine **5** (0.01 mol) in ethanol (30 mL) was refluxed for 10 h. To obtain 2-(furan-2-yl)-4(3*H*)-substituted quinazolin-4-ones (**6a-f**), the reaction mixture was concentrated to half its volume and the separated solid was filtered, washed with distilled water and recrystallized with ethanol. The TLC was performed on silica gel G-plates using cyclohexane:ethyl acetate (2:1) to assess the purity and homogeneity of the compounds (**Scheme-I**).

2-(Furan-2-yl)-4-oxoquinazoline-3(4*H*)-carboximidamide (6a): Yield, 78%: m.p.: 159-164 ºC; FT-IR (KBr, ν_{max}, cm^{-1}): 3277 (N-H *str.*), 1705 (C=O), 1647 (C=N), 1139 (C-O-C), 1062 (3°N); ^{1}H NMR (DMSO-d_6, δ ppm): 8.21 (d, 1H), 7.45 (m, 1H), 7.42 (m, 1H), 7.51 (d, 1H), 7.26 (d, 1H), 6.62 (s, 1H), 7.93 (s, 1H), 9.91 (s1H, NH), 5.73 (s, 2H, NH_2); MS (*m/z*, %): 255.33 (M^+). Anal. calcd. (found) % for $C_{13}H_{10}N_4O_2$: C, 61.41 (61.64); H, 3.96 (4.05); N, 22.04 (21.99); O, 12.59 (12.38).

***N*-(*N*,*N*-Dimethylcarbamimidoyl)-2-(furan-2-yl)-4-oxoquinazolin-3(4*H*)-carboximidamide (6b):** Yield, 79%: m.p.: 197-202 ºC; FT-IR (KBr, ν_{max}, cm^{-1}): 1685 (C=O), 1641 (C=N), 1161 (3°N), 1087 (C-O-C), 1605 (-CH_3); ^{1}H NMR (DMSO-d_6, δ ppm): 8.06 (d, 1H), 7.45 (m, 1H), 7.42 (m, 1H), 7.51 (d, 1H), 7.27 (s, 1H), 6.74 (d, 1H), 7.98 (s, 1H), 8.6 (d, 2H=NH), 12.3 (s, 1H, NH), 2.67 (s, 6H, CH_3); MS (*m/z*, %): 325.72 (M^+). Anal. calcd. (found) % for $C_{16}H_{16}N_6O_2$: C: 59.25 (59.11); H, 4.97 (4.85); N, 25.91 (25.99); O, 9.87 (10.08).

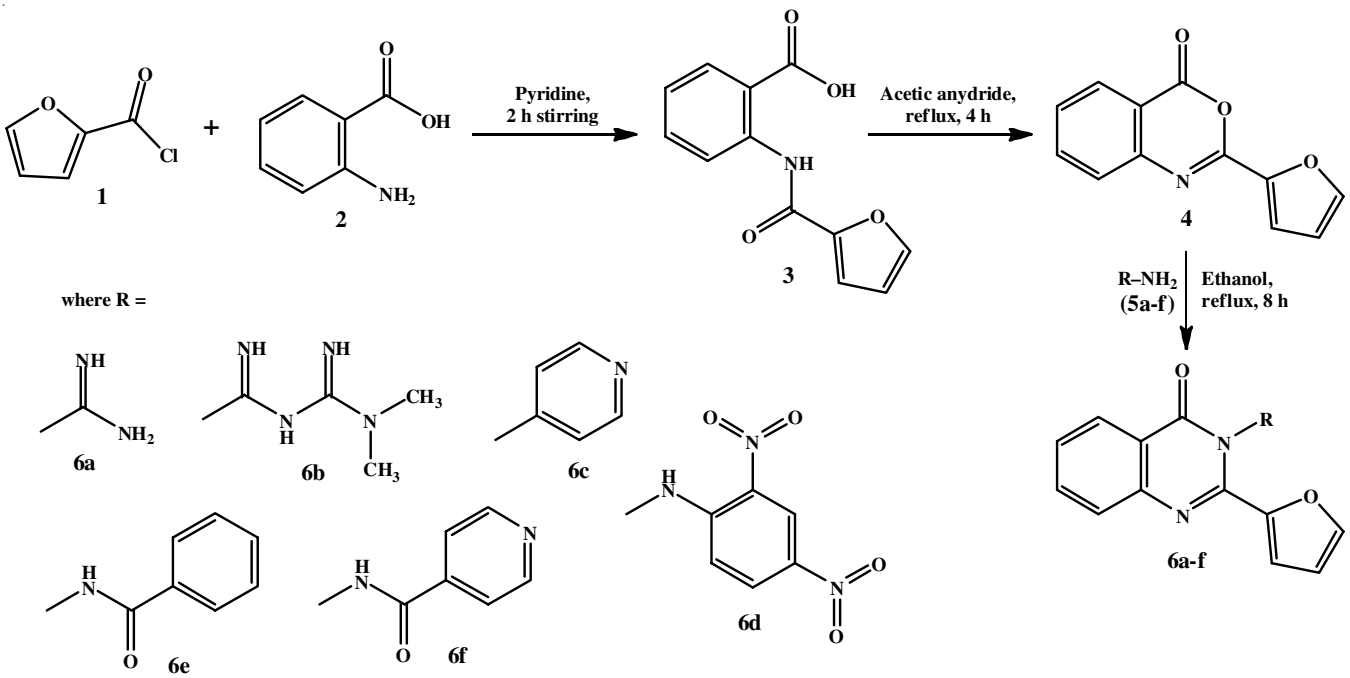

Scheme-I: General synthetic route for 2-furanyl-3-substituted quinazoline-4-one derivatives (**6a-f**)

2-(Furan-2-yl)-3-(pyridin-2-yl)quinazolin-4 (3*H*)-one (6c): Yield, 75%: m.p.: 186-189 ºC; FT-IR (KBr, ν_{max}, cm^{-1}): 1732 (C=O), 1702 (C=N), 1142 (3°N), 1138 (C-O-C); ^{1}H NMR (DMSO-d_6, δ ppm): 8.23 (d, 1H), 7.44 (m, 1H), 7.41 (m, 1H), 7.5 (d, 1H), 7.26 (d, 1H), 6.62 (d, 1H), 7.93 (s, 1H), 7.9 (s, 1H), 7.85 (m, 1H), 7.21 (m, 1H), 8.44 (m, 1H); MS (*m/z*, %): 290.61 (M^+). Anal. calcd. (found) % for $C_{17}H_{11}N_3O_2$: C, 70.58 (70.66); H, 3.83 (3.95); N, 14.53 (14.69); O, 11.06 (10.98).

3-[(2,4-Dinitrophenyl)amino]-2-(furan-2-yl)quinazolin-4 (3*H*)-one (6d): Yield, 82%: m.p.: 225-228 ºC; FT-IR (KBr, ν_{max}, cm^{-1}): 1662 (C=O), 1568 (C=N), 1537 (NO_2), 1326 (2°N), 1094 (C-O-C), 1078 (3°N); ^{1}H NMR (DMSO-d_6, δ ppm): 8.05 (d, 1H), 7.43 (m, 1H), 7.41 (m, 1H), 7.49 (d, 1H), 7.26 (d, 1H), 6.62 (s, 1H), 7.93 (s, 1H), 8.75 (d, 1H), 8.42 (d, 1H), 7.96 (d, 1H), 6.33 (s, 1H, NH) ppm; MS (*m/z*, %): 394.23 (M^+). Anal. calcd. (found) % for $C_{18}H_{11}N_5O_6$: C, 54.97 (55.02), H, 2.82 (2.91); N, 17.81 (17.79); O, 24.41 (24.47).

***N*-[2-(Furan-2-yl)-4-oxoquinazolin-3(4*H*)-yl]benzamide (6e):** Yield, 81%: m.p.: 245-248 ºC; FT-IR (KBr, ν_{max}, cm^{-1}): 1678 (C=O), 1649 (C=N), 1294 (2°N), 1055 (C-O-C), 1103 (3°N); ^{1}H NMR (DMSO-d_6, δ ppm): 8.23 (d, 1H), 7.43 (m, 1H), 7.41 (m, 1H), 7.49 (d, 1H), 7.26 (d, 1H), 7.24 (s, 1H), 6.62 (d, 1H), 7.96 (d, 1H), 8.0 (t, 2H), 7.58 (d, 2H), 6.34 (s, 1H, NH); MS (*m/z*, %): 332.45 (M^+). Anal. calcd. (found) % for $C_{19}H_{13}N_3O_3$: C, 68.88 (68.93); H, 3.95 (4.05); N, 12.68 (12.59); O, 14.49 (14.54).

***N*-[2-(Furan-2-yl)-4-oxoquinazolin-3(4*H*)-yl]pyridine-4-carboxamide (6f):** Yield, 79%: m.p.: 206-210 ºC; FT-IR (KBr, ν_{max}, cm^{-1}): 1666 (C=O), 1643 (C=N), 1304 (2°N), 1174 (ArC-N-C), 1084 (3°N), 1043 (C-O-C); ^{1}H NMR (DMSO-d_6, δ ppm): 8.23 (d, 1H), 7.43 (m, 1H), 7.41 (m, 1H), 7.49 (m, 1H), 7.26 (d, 1H), 6.62 (d, 1H), 7.93 (s, 1H), 7.86 (m, 2H), 8.72 (d, 2H), 6.35 (s, 1H, NH); MS (*m/z*, %): 333.52 (M^+). Anal. calcd. (found) % for $C_{18}H_{12}N_4O_3$: C, 65.06 (65.15); H, 3.64 (3.75); N, 16.86 (16.81); O, 14.44 (14.49).

Anti-tubercular activity: The synthesized quinazolinone derivatives (**6a-f**) were screened for their anti-tubercular activity using MABA method [17]. For this reason, the efficacy of six quinazolinone derivatives were screened against the Mtb H37RV strain in Middlebrook 7H9 (MB 7H9) broth using three standard drugs *viz*. streptomycin (6.25 mg/mL), pyrazinamide (3.125 mg/mL) and ciprofloxacin (3.125 mg/mL). To prevent medium from evaporating from test wells during incubation, 200 µL of sterile deionized water was applied to the outside perimeter wells of a sterile 96 wells plate. About 100 µL of MB 7H9 broth was added to the 96-well plate and the compounds were diluted serially there. Parafilm was used to cover and seal the plates before they were placed in a 37 ºC incubator for 5 days. The plate was incubated for another 24 h and then 25 µL of 1:1 alamar blue reagent and 10% Tween 80 was added. A blue colour meant there were no bacteria, while a pink colour meant there were some growth [18].

Molecular docking

Preparation of macromolecule: The 3D crystal structure of *Mtb*InhA in complex with 2-(*o*-tolyloxy)-5-hexylphenol (PT70) was retrieved from the RCSB protein data bank(PDB code: 2X23). Inhibitor of InhA activity is PT70, which binds slowly and tightly [19]. To find and develop novel inhibitors that exhibit long residence time with InhA, the PT70-induced conformation was used. ModRefiner, a web-based application was used to refine the model. ModRefiner minimized the protein's energy by selecting the residues from the permissible region. The online RAMPAGE programme was used to generate a Ramachandran plot, which was then used to evaluate and validate the models. The protein was further validated using the online SAVES version 4.

The LigX panel in MOE was used for the preparation of the protein, as it provides an automated process for structural correction, protonation, tethering and minimization stages of structure preparation. The default setting of LigX panel was applied [gradient: 0.0001RMS kcal/mol/Å, force field: MMFF94x, atoms further than 8 Å from the ligand were fixed, hydrogen atoms close to the ligand were not fixed].The site finder panel, on the other hand, was used to identify the binding site of the target protein.

The first step in a rigid protein docking studies using FORECASTER is to add hydrogen atoms, generate the possible tautomers and optimize the hydrogen bond network using Protein Rotamers Elaboration and Protonation based on Approximate Residue (PREPARE).The ligand was identified in order to define the active site. Protein conformational ensemble system setup (PROCESS) was used to setup the protein for docking studies.

Ligands preparation: With the help of ChemSpider Version 2022.0.55.0, the 2D chemical structures of the ligands were prepared [20]. The 2D chemical structures (SD file) were imported into MOE database, which was visually inspected for bonding patterns and altered in order to correct any structure drawing error. Eventually, the ligands were minimized using MMFF94x force field and a gradient of 0.0001 RMS kcal/mol/Å. During the energy minimization, hydrogen atom was added and the atomic partial charges were calculated using the same force field.

For FITTED docking studies, the 2D structures of the ligands were converted into 3D structures using Conformational Optimization of Necessary Virtual Enantiomers, Rotamers and Tautomers (CONVERT). Then, Small Molecule Atom Typing and Rotatable Torsions (SMART) was used for setting the atomic partial charges of the ligands using DGH.

Docking validation: UCSF Chimera for Mac was used to remove the ligand from the active site of crystal structure of InhA [21]. After re-docking the ligand, MacPyMOL was used to align the docked ligand with ligand from the crystal structure [22].

Docking studies: Docking simulation was performed using MOE 2014.0901 software package. In the docking studies, several binding poses were obtained for each compound using a triangle matcher placement method. The scores assigned to each generated poses by the placement method were re-scored using London dG, which estimated the free energy of binding of the ligand from the given pose. Thirty poses were retained from the placement stage, which were refined using MMFF94x force field. The binding pose with the highest final score was

regarded to be the ligand's binding affinity value, when the final refined poses were re-scored using the GBVI/WSA dG force field-based scoring procedure. Additional docking studies was performed using flexibility induced through targeted evolutionary description (FITTED). During the studies, the RMSD value of the docked conformer with respect to the crystal conformer of PT70 was also calculated.

RESULTS AND DISCUSSION

Compounds **6a-f** were synthesized by condensation of 2-(furan-2-yl)-4(3*H*)-1-benzoxazin-4-one with primary amines in ethanol in mild experimental conditions and the yields were satisfactory. All the synthesized compounds were confirmed using the analytical and spectral data from FT-IR, ^{1}H NMR and mass analysis.

Anti-tubercular activity: Using microplate alamar blue assay (MABA) method, all the synthesised quinazolinones (**6a-f**) were evaluated for their anti-tubercular activity. Among the synthesized quinazolinones, compounds **6c** and **6d** were found to be more potent. In addition, compounds **6a**, **6b** and **6e** were found to be moderately potent, as they exhibited MIC at 50 µg/mL. In contrary to the these compounds, compound **6f** show low activity at 100 µg/mL (Table-1).

Compound **6c** is an isostere analogue of 2-furan-2-yl-3-phenyl-3*H*-quinazolin-4-one, where pyridine is used instead of a phenyl group. Fortunately, this isosteric replacement is associated with higher anti-tubercular activity, which explains the importance of having a side chain with higher hydrogen bond acceptor property.

Molecular docking: The target crystal structure was refined using ModRefiner refinement server [23]. For the synthesized compounds, RAMPAGE software [24] is used generated a Ramachandran plot, a standard method for evaluating protein structural quality. Almost all (97.3%) of the residues fell inside the permitted zone, whereas only 2.3% were outside it. Also, in the outlier region, there were no residues (Fig. 1).

The protein structure was also validated and checked using Structural Analysis and Verification Server (SAVES) version 4 [25]. The average 3D-1D score for residues in VERIFY3D was found to be 95.15% of the residues had an averaged score of ≥ 0.2. When compared to the pass value of at least 80% of amino acids with a score of ≥ 0.2 in the 3D-1D profile, this value is found to be higher. The modified molecule likewise passed the PROOF verification procedure.

The binding site of InhA for MOE docking was identified using its site finder panel [26]. MOE's site finder is a validated geometric method since no energy models are used. In lieu of

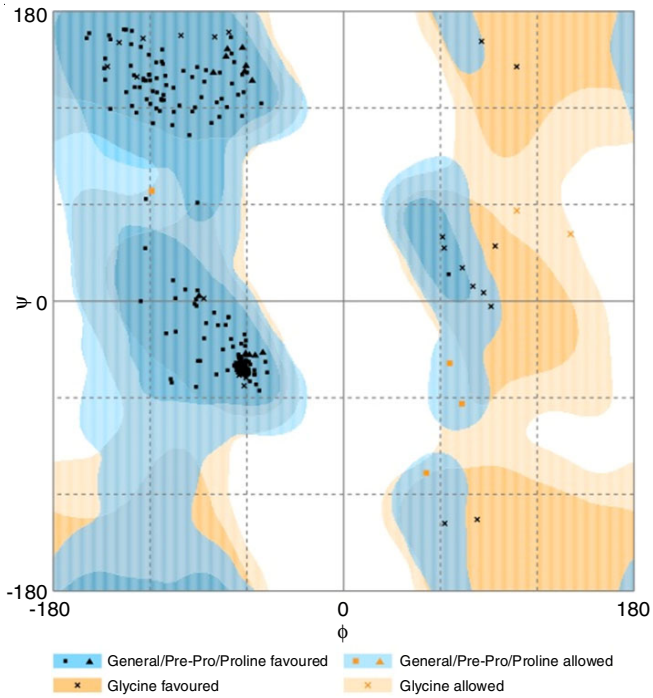

Fig. 1. Ramachandran plot for the analysis of ψ and ϕ torsion angles for all residues of the refined macromolecule

energy models, the relative locations and accessibility of the receptor atoms, as well as a basic classification of the chemical kind, are evaluated. Site finder generated eighteen possible binding sites, of which the first generated site which contains Gly14, Ile15, Ile16, Thr17, Ser20, Ile21, Ala22, Thr39, Gly40, Phe41, Asp42, Arg43, Ile47, His93, Ser94, Ile95, Gly96, Phe97, Pro99, Gln100, Met103, Ile122, Met147, Asp148, Phe149, Asp150, Pro151, Ser152, Arg153, Ala154, Met155, Pro156, Ala157, Tyr158, Met161, Lys165, Ala191, Gly192, Ala190, Pro193, Ile194, Thr196, Lue197, Ala198, Met199, Ala201, Ile202, Val203, Leu207, Gln214, Ile215, Leu217, Ile218, Gly221, Tyr259, Asp261, Ala264, His265, Gln267 and Leu268 was selected (Fig. 2). On the other hand, the active site in FITTED docking was defined as a region around PT70 ligand.

Prior to docking of the synthesized quinazolinones, the MOE docking simulation was validated. Hence, analysis revealed that the X-ray crystallographic conformer is similar to the docked conformer, as determined from the alignment of the two structures with an RMSD value of 1.529 Å (Fig. 3).

The optimal binding geometries and energies of each ligand against InhA macromolecule were calculated using MOE's

TABLE-1
ANTI-TUBERCULAR ACTIVITY (MIC VALUES AND THE BINDING AFFINITIES TO InhA) OF QUINAZOLINONE DERIVATIVES

Compounds	*M.tuberculosis* $H_{37}RV$ MIC (µg/mL)	Binding affinity (Kcal/mol) from MOE	FORECASTER suite	
			Binding affinity (Kcal/mol)	RMSD
6a	50	-5.87	-13.20	7.25
6b	50	-6.81	-11.71	8.12
6c	12.5	-6.66	-7.72	8.90
6d	25	-7.37	-10.62	7.89
6e	50	-6.88	-9.30	5.81
6f	100	-7.15	-10.84	8.64

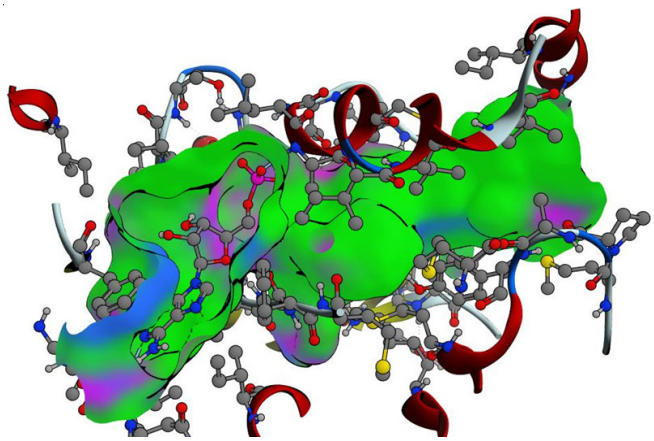

Fig. 2. Possible binding site of InhA calculated by MOE's site finder

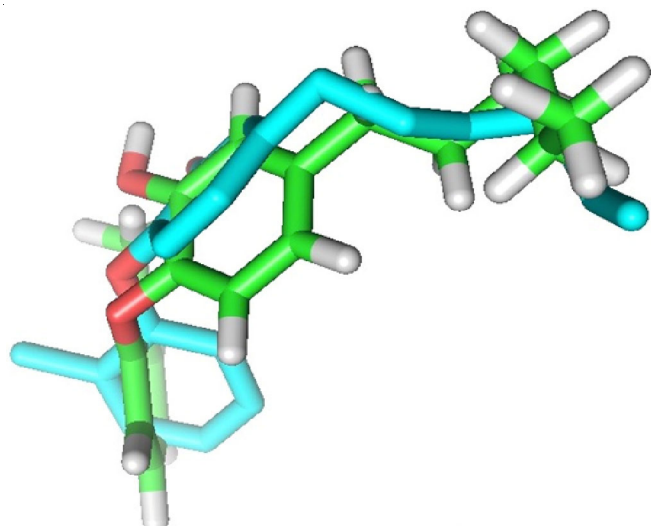

Fig. 3. Alignment of the docked ligand (cyan) on the X-ray crystal ligand (green) in the active site of InhA

dock application and FORECASTER drug suite, which are among the most effective docking techniques. In MOE docking procedure, the binding poses with the highest score were considered as the binding affinity value of the ligand (Table-1). Accordingly, compound **6d** (-7.37 Kcal/mol) and compound **6f** (-7.15 Kcal/mol) showed the highest binding score among the synthesized analogues. The lowest binding score, on the other hand, was exhibited by compound **6a** (-5.87 Kcal/mol). The docking scores from FITTED were different from those found in MOE docking. In FITTED docking, compound **6a** (-13.20 Kcal/mol) showed the highest binding affinity, which is followed by compound **6b** (-11.71 Kcal/mol) and compound **6f** (-10.84 Kcal/mol).

A good correlation could not be found between docking scores from both docking simulations and MIC values, which is observed from a correlation factor coefficient value less than 0.03. Nonetheless, this discrepancy is to be expected given the complexity of MIC values, which involve not just target inhibition but also a number of other processes. Compound **6b**, for example, exhibited lower anti-tubercular activity (MIC = 50 µg/mL) but a higher docking scores in both docking tools used. The lower MIC value may be due to the possible ionization of the biguanide group, which might decrease the ability to cross the lipophilic cell membrane of *M. tuberculosis* $H_{37}RV$. On the other hand, the docking analysis showed a hydrogen bond interaction between biguanide moiety and InhA.

The amino acids that interact with the synthesized quinazolinone derivatives (**6a-f**), as obtained from the MOE docking, clearly shows that the synthesized analogues used common amino acids for their interaction with InhA (Table-2). Moreover, Gly14, Ser94, Ile202 and Val203 were found to interact with nearly all of the synthesized quinazolinone derivatives.

A simplified 2D binding interactions and 3D interactions between the top four most active compounds from the MOE docking (compounds **6b**, **6e** and **6f**) and InhA are given in Table-3. The side chains of compound **6a**, **6b**, **6e** and **6f** were involved in the hydrogen bonding interactions.

Conclusion

In present work, a new series of 2-furanyl-3-substituted quinazolin-4-one derivatives (**6a-f**) were synthesized and characterized. Most of the synthesized compounds exhibited a promising anti-tubercular activity. Among the series, 2-(furan-2-yl)-3-(pyridin-2-yl)quinazolin-4 (3*H*)-one (**6c**) and 3-[(2,4-dinitrophenyl)amino]-2-(furan-2-yl)quinazolin-4(3*H*)-one (**6d**) emerged as the most active as they show MIC value of 12.5 and 25 µg/mL, respectively. According to the structural activity relationship studies, by substituting pyridine or 2,4-dinitroaniline at position 3 of 2-furanyl quinazolinone can increase anti-tubercular activity. Further research on analogues with a different amide or pyridine substituent at position 3 could result in far more potent anti-tubercular agents. Aromatic side chain with substituent capable of forming hydrogen bond interactions is found to increase the affinity to InhA molecule. Unfortunately, a poor correlation was found between anti-tubercular activities and docking scores of the synthesized compounds. Considering a moderate binding affinity, InhA structure based

TABLE-2
SUMMARY OF THE AMINO ACIDS INTERACTING WITH QUINAZOLINONE DERIVATIVES

Compounds	HB interactions	Hydrophobic interactions
6a	T196, I21 H-arene	G14, S20, S94, I95, G96, M147, D148, F149, K165, G192, P193, I194, A198, M199
6b	S94	G14, S20, I21, A22, I95, G96, F97, M98, M103, M147, F149, Y158, M161, A191, G192, P193, T196, I202, V203
6c		I21, S94, I95, G96, F97, M98, M103, Y158, D148, K165, M147, F149, M161, A191, G192, P193, I194, A198, I202, V203
6d	A198 H-arene	G14, I16, S20, I21, A22, S94, I95, G96, F97, M147, K165, L197, A198, I202
6e	I95, G96 (2*)	G14, I16, S20, F41, L63, V65, S94, I21, I122, L197, A198, I202
6f	Y158 H-arene, T196	G14, I16, S20, I21, A22, S94, G96, F97, M98, M103, F149, M161, A191, G192, P193, A198, M199, I202, V203

TABLE-3
A 2D AND 3D INTERMOLECULAR INTERACTIONS OF THE TOP FOUR MOST ACTIVE COMPOUNDS

Compounds	Simplified 2D interactions	3D representation
6b	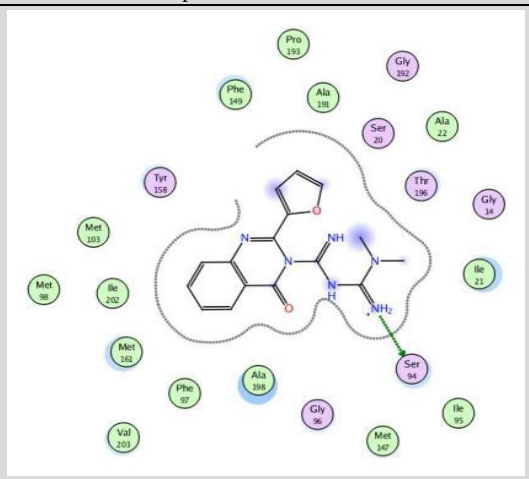	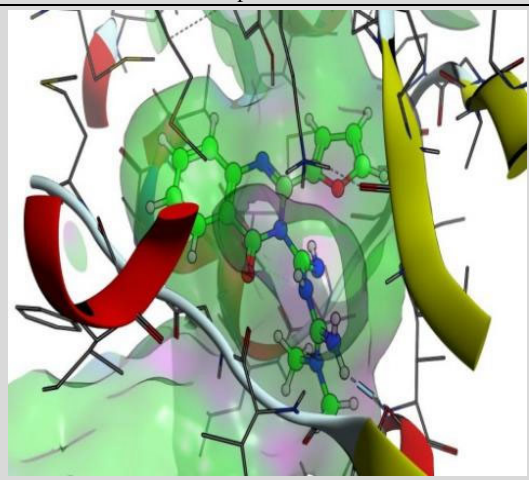
6e	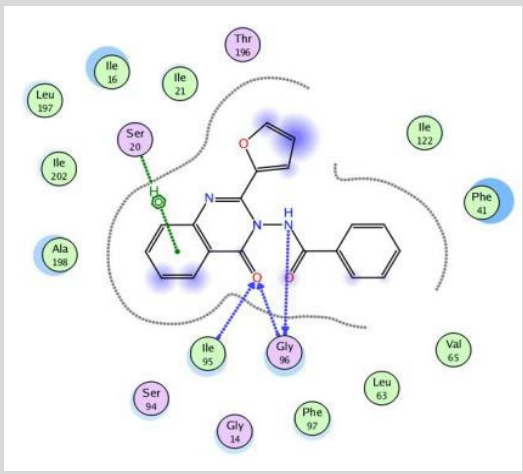	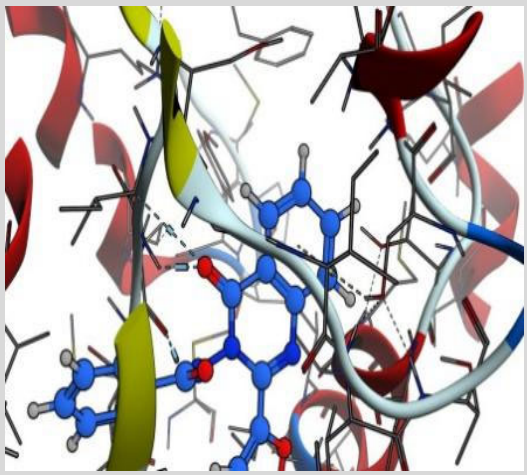
6f	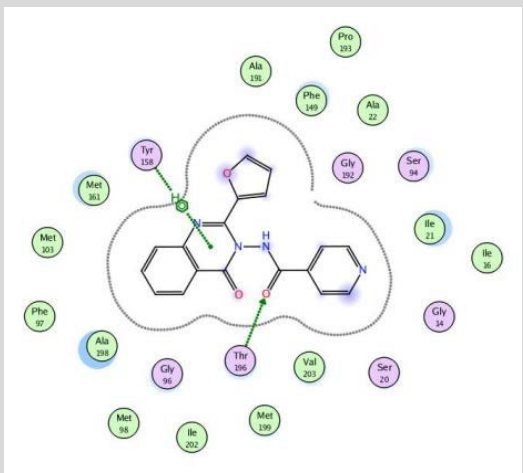	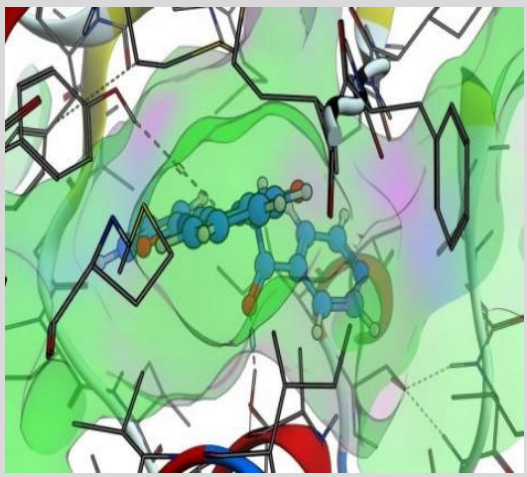

The green circles show hydrophobic amino acids; the purple circles show polar amino acids; the blue regions on the ligand show regions exposed to solvent; the broken green arrow shows side chain acceptor; the broken blue arrow shows backbone donor.

design of 2-furanyl quinazolinone scaffold may lead to more potent and selective anti-tubercular agents.

ACKNOWLEDGEMENTS

The authors are grateful to Sri Padmavathi School of Pharmacy for providing the research facilities. The authors are also grateful for the authorities of UCSF chimera and PyMOL for providing free software.

CONFLICT OF INTEREST

The authors declare that there is no conflict of interests regarding the publication of this article.

REFERENCES

1. WHO, Global Tuberculosis Report 2021, World Health Organization, Edn. 26 (2021).
2. A.A. Velayati, M.R. Masjedi, P. Farnia, P. Tabarsi, J. Ghanavi, A.H. ZiaZarifi and S.E. Hoffner, *Chest*, **136**, 420 (2009); https://doi.org/10.1378/chest.08-2427
3. Y. Xi, W. Zhang, R.-J. Qiao and J. Tang, *PLoS ONE*, **17**, e0270003 (2022); https://doi.org/10.1371/journal.pone.0270003
4. Z.F. Udwadia, R.A. Amale, K.K. Ajbani and C. Rodrigues, *Clin. Infect. Dis.*, **54**, 579 (2012); https://doi.org/10.1093/cid/cir889
5. Z.F. Udwadia, *J. Assoc. Chest Physicians*, **4**, 41 (2016); https://doi.org/10.4103/2320-8775.183836
6. A. Allué-Guardia, J.I. García and J.B. Torrelles, *Front. Microbiol.*, **12**, 612675 (2021); https://doi.org/10.3389/fmicb.2021.612675
7. K.J. Seung, S. Keshavjee and M.L. Rich, *Cold Spring Harb. Perspect. Med.*, **27**, a017863 (2015); https://doi.org/10.1101/cshperspect.a017863
8. A. Zumla, P. Nahid and S.T. Cole, *Nat. Rev. Drug Discov.*, **12**, 388 (2013); https://doi.org/10.1038/nrd4001
9. R. Karan, P. Agarwal, M. Sinha and N. Mahato, *ChemEngineering*, **5**, 73 (2021); https://doi.org/10.3390/chemengineering5040073
10. J.N. Akester, P. Njaria, A. Nchinda, C.L. Manach, A. Myrick, V. Singh, N. Lawrence, M. Njoroge, D. Taylor, A. Moosa, A.J. Smith, E.J. Brooks, A.J. Lenaerts, G.T. Robertson, T.R. Ioerger, R. Mueller and K. Chibale, *ACS Infect. Dis.*, **6**, 1951 (2017); https://doi.org/10.1021/acsinfecdis.0c00252
11. A.K. Khan, *Al-Mustansiriyah J. Sci.*, **28**, 122 (2018); https://doi.org/10.23851/mjs.v28i3.180
12. E. Jafari, M.R. Khajouei, F. Hassanzadeh, G.H. Hakimelahi and G.A. Khodarahmi, *Res. Pharm. Sci.*, **11**, 1 (2016).
13. K.K. Rajasekhar, N.D. Nizamuddin, A.S. Surur and Y.T. Mekonnen, *Res. Rep. Med. Chem.*, **6**, 15 (2016); https://doi.org/10.2147/RRMC.S91474
14. D. Rozwarski, C. Vilcheze, M. Sugantino, R. Bittman and J. Sacchettini, *J. Biol. Chem.*, **22**, 1582 (1999).
15. C. Vilchèze and W.R. Jacobs Jr., *Annu. Rev. Microbiol.*, **61**, 35 (2007); https://doi.org/10.1146/annurev.micro.61.111606.122346
16. R.P. Massengo-tiasse and J.E. Cronan, *Cell. Mol. Life Sci.*, **66**, 1507 (2009); https://doi.org/10.1007/s00018-009-8704-7
17. S.G. Franzblau, R.S. Witzig, J.C. McLaughlin, P. Torres, G. Madico, A. Hernandez, M.T. Degnan, M.B. Cook, V.K. Quenzer, R.M. Ferguson and R.H. Gilman, *J. Clin. Microb.*, **36**, 362 (1998); https://doi.org/10.1128/JCM.36.2.362-366.1998
18. S.G. Franzblau, R.S. Witzig, J.C. McLaughlin, P. Torres, G. Madico, A. Hernandez, M.T. Degnan, M.B. Cook, V.K. Quenzer, R.M. Ferguson and R.H. Gilman, *J. Clin. Microbiol.*, **36**, 362 (1998); https://doi.org/10.1128/JCM.36.2.362-366.1998
19. X. He, A. Alian, R. Stroud and P.R. Ortiz de Montellano, *J. Med. Chem.*, **49**, 6308 (2006); https://doi.org/10.1021/jm060715y
20. http://www.chemspider.com/Chemical-Structure.1906.html. Version 2022.0.55.0, Royal Society of Chemistry 2022, 207890.
21. E. Pettersen, T. Goddard, C. Huang, G. Couch, D. Greenblatt, E. Meng and T. Ferrin, *J. Comput. Chem.*, **25**, 1605 (2004); https://doi.org/10.1002/jcc.20084
22. The PyMOL Molecular Graphics System, version 1.7.4 Schrödinger, LLC.
23. D. Xu and Y. Zhang, *J. Biophys.*, **101**, 2525 (2011); https://doi.org/10.1016/j.bpj.2011.10.024
24. S.C. Lovell, I.W. Davis, W.B. Arendall III, P.I.W. de Bakker, J.M. Word, M.G. Prisant, J.S. Richardson and D.C. Richardson, *Proteins*, **50**, 437 (2003); https://doi.org/10.1002/prot.10286
25. http://nihserver.mbi.ucla.edu/SAVES/ (2011).
26. Molecular operating environment (MOE), 2013.08, Chemical Computing Group Inc., Montreal, QC, Canada, H3A 2R7(2015).